A SIMULATION TOOL FOR EVALUATING THE THERMAL VIABILITIES OF PHASE-II CMS FORWARD PIXEL DETECTOR ASSEMBLIES

A Thesis

Presented to the Faculty of the Department of Physics

of Cornell University

in Partial Fulfillment of the Requirements for the Degree of

Bachelor of Arts

by

Arthur Campello

May 2020

A SIMULATION TOOL FOR EVALUATING THE THERMAL VIABILITIES OF PHASE-II CMS FORWARD PIXEL DETECTOR ASSEMBLIES

Arthur Campello, B.A.

Cornell University 2020

This thesis outlines the development, testing, and use of a flexible and robust thermal simulation tool for comparative thermal evaluations of various assembly designs involving particle trackers known as "modules." The tool is aimed at conceptually guiding designs for an upgraded assembly of the forward pixels of the Compact Muon Solenoid (CMS) detector's inner tracker. This new design is a part of the Phase-II CMS upgrade in preparation for the high-luminosity Large Hadron Collider (HL-LHC) to begin operations in 2027. The thesis begins with a complete description of the design problem, including the constraints faced by the design and it's current state. It proceeds to outline the reasons a ground-up finite-difference thermal simulation tool serves better than either analytical calculations or industrial thermal software to guide the early stages of thermal design. From here, the thesis includes a thorough description of ways to numerically model heat flow dynamics, involving various types of thermal components and materials, using finite difference approximations. A chapter detailing the computational methods behind executing the calculations is also included. From here, the thesis details how the problem at hand is implemented into the framework described in earlier chapters and how evaluation criterion are determined. Finally, it describes the results of several simulations performed to compare various sets of general designs and includes a discussion on the performance of the tool, the uncertainties involved in the problem, and the future of the tool's use for detector mechanics research.

Biographical Sketch

Arthur Campello grew up in Champaign, Illinois, a child of Brazilian immigrants, and graduated from Lansing High School in Lansing, New York in 2015. Upon graduation, he worked for a year as a mechanical design intern at the Cornell High Energy Synchrotron Source (CHESS) and enrolled in Cornell University in 2016. At Cornell, Arthur has completed the required coursework for the physics major and is expected to graduate with an additional major in economics. He additionally spent the summer of 2019 as a research support intern at the SLAC National Accelerator Laboratory. After graduation he plans enroll as a PhD student at Stanford University, where he as accepted an offer of admission from the Department of Applied Physics.

Acknowledgements

I would first like to acknowledge my thesis supervisor Professor Jim Alexander, who sagely guided me through my research related to this work and through most of my undergraduate research and academic careers. His insightful advice over the past few years made this thesis possible and helped me make critical decisions through my journey as an early scientist. I would also like to acknowledge Dr. José Monroy and Yadira Bordlemay Padilla for their close supervision of my work related to the Phase-II CMS upgrade project over the past few years. With them I include the other current and former students collaborating with the CMS mechanics group at Cornell, especially Neil Minet, with whom I have worked closely. At my internship at SLAC over the summer, staff scientist Andy Aquila enabled my development of the computational skills critical to completing this work. My research supervised by CHESS staff scientist Stanislav Stoupin additionally taught me to confidently exercise scientific writing and strengthened my abilities in coding with Python. Additionally, I would like to thank Professor Carl Franck for his academic supervision through my freshman and sophomore years as an undergraduate. His guidance strengthened my abilities as an experimentalist and introduced me to scientific writing in physics. Finally, I acknowledge Statistics Professor Thomas DiCiccio, whose supervision of my research in statistics taught me to explore new approaches to natural puzzles and how to make concrete mathematical statements.

Table of Contents

List of Tables

List of Figures

Chapter 1

Introduction

The Compact Muon Solenoid (CMS) experiment is a 14,000-tonne general-purpose particle detector housed at one of the collision points of the Large Hadron Collider (LHC) at the CERN Laboratory in Geneva, Switzerland [CERN CMS]. It was instrumental in the discovery of the Higgs Boson in 2012 [Chatrchyan *et al.*, 2012] and remains in operation today, with the aim of uncovering new physics. The fundamental mechanism by which the CMS detects particles created during a proton-proton collision generated by the LHC follows two steps. The particles first travel through tightly-spaced silicon trackers which generate information about the trajectory of the particles. The particles then reach various calorimeters which record the energies of the outgoing particles to identify them. From these stages, an almost complete set of information is generated about the particles created from the high-energy interactions between the quarks and gluons of the incoming protons. Since the 2012 detection of the Higgs Boson, the European Strategy Group pointed to the importance of increasing the "luminosity" of the LHC (i.e. the

number of protons in a collision) in the effort to learn more about the Higgs and uncover physics beyond the standard model. With this in mind, CERN launched the "High-Luminosity" LCH (HL-LHC) project with an aim to increase the luminosity of the current LHC by a factor of 10 for experiments in 2027 [CERN LHC].

Unfortunately, the CMS detector currently present at the LHC is unable to survive the high about of radiation generated by the planned HL-LHC and, survival aside, it cannot efficiently detect the increased number of event rates [Contardo *et al.*, 2015]. Thus, CMS collaborators across hundreds of institutions put forward a proposal to upgrade the current CMS detector to a version that can survive the higher doses of radiation, effectively detect higher event rates, and incorporate new technologies and benefits not present in the existing detector. This effort is known as the Phase-II Upgrade of the CMS. Among these institutions is Cornell University, whose mechanics group has been tasked with developing and constructing the forward-pixel detectors of the inner tracker of the detectors. The figure below shows a quarter cross-section of the proposed silicon tracker structure of the new detector with the forward pixels shown as green vertical lines.

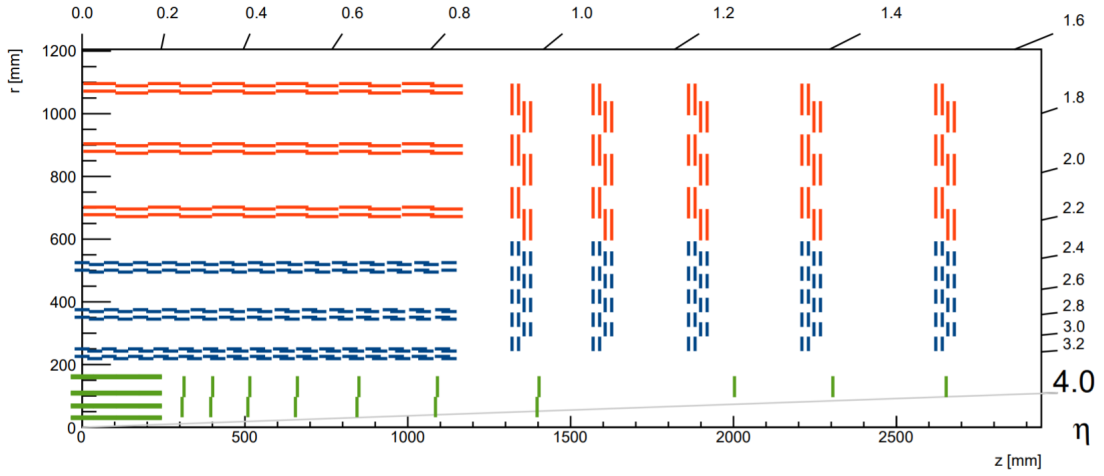

Figure 1.1: A sketch of one quarter of the tracker layout with the Inner Pixel detectors shown in green and the Forward Pixel detectors shown as vertical green lines [Contardo *et al.*, 2015]

Assuming all particles originate from the collision point, shown as the $(0, 0)$ coordinate in Figure 1.1, the majority of the particles impinging on the forward-pixel detectors will do so perpendicularly to their planar components. Thus, it is optimal for the forward pixel detector to position its silicon tracking units close to parallel to its surfaces. Within mechanics groups, and from here in the thesis, these individual silicon-comprised particle tracking units are called "modules." In addition to being placed flat against the detector planes, the modules must also be arranged such that they form an almost complete covering over the paths a particle could take from the collision point (with the exception of those of pseudorapidities of over $\eta = 4$ as shown in Figure 1.1). This means that the forward pixel detector must be made of very many silicon-based modules placed closely together to avoid the possibility that particles miss passing through them.

As these modules must be powered and continuously read out events at high rates, they require connections to power supplies and read-out chips with attachments to fiber-optic components. With these constraints alone, the problem of constructing the forward pixel detector is already made difficult. Unfortunately, however, the design of the detector is made even more challenging by the fact that the new modules will operate at much higher power levels than those from the earlier iteration of the detector. This is needed so that the Phase-II-upgraded detector can fulfill its goal of sufficient event detection rates for the HL-LHC. Currently, it is estimated that the modules will receive approximately 2.5 Watts of power each. At this power level, it is likely that an individual module alone in air would overheat and fail to function without some cooling system. In the realistic scenario of many modules packed close together in air with no cooling system – restricting airflow in the process – the entire detector would likely fail. For this reason, the current forward pixel detector will be built with cooling in mind. Specifically, each

semi-cylindrical half of it will be made of stacked semi-circular disks known as "dees" on which the modules will be mounted (on both sides with offsets to ensure full detection of particles). Through the dees will run a cooling tube (made either of stainless steel or titanium) that carries CO_2 in liquid form. The tube will follow an "antler" pattern such that most (if not all) modules have two tube-contacts running along their surfaces. The figure below shows a model of the arrangements of these modules on the dee in the left and a model of the tubing shape within the dee on the right.

a) b)

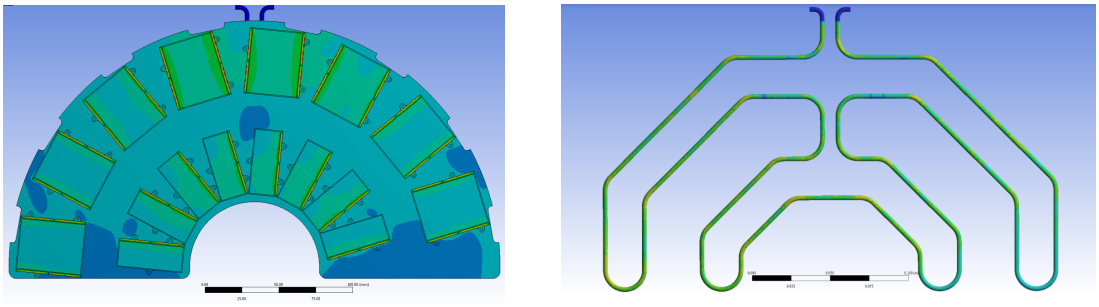

Figure 1.2: a). A model of a dee with modules (shown as rectangles) mounted on it. The inlet and outlet of the tube can be seen protruding from the top of the dee. b). A model of the cooling tubing that passes through the dee. Note that the shape of this tubing corresponds to that which passes as close as possible to the most number of modules. These images were taken from screen-captures of the thermal simulation software ANSYS®. Credit to Samuel Bright-Thonney.

It is expected that the liquid CO_2 will be kept at a temperature of -30° Celsius and may undergo a phase transition to a gas as it passes through the dee due to the heat imparted on it from the modules. While this addition to the design greatly facilitates cooling, there remains a possibility that the components in between the heated elements of the module and the cooling tube will prevent the cooling tube from drawing enough heat away from the module to avoid a "thermal runaway" scenario, where all modules simultaneously overheat and the entire detector is

destroyed. Though materials of high thermal conductivities (such as common metals) would solve this issue, other constraints on the detector design make such trivial solutions unfeasible. Among the most important of such constraints is that components used in the detector must be both "low-Z" and "radiation-hard." This means that the particles must not lose energy when interacting with the materials (as this would compromise the overall detection ability of the experiment) and that the materials must not degrade with radiation under the added dosage present in the high-luminosity LHC. The former constraint rules out thick metals. In addition to this, the overall assembly of the detector must be made as light as possible to avoid deformation of detector components, which would compromise the reconstruction of particle paths from tracker data. Finally, the components must be fairly inexpensive to avoid budget overruns.

Of great concern to the Cornell CMS mechanics group and to this thesis is the ability of the detector assembly to avoid thermal runaway, i.e. to remain "thermally viable." As this is a binary categorization of a design that, if not met, means the design fails entirely, it is easy to prioritize it as one of utmost concern. An additional reason for specific focus on this quality of a design is that it is more difficult to estimate than all others. As members of a physics department, the collaborators of Cornell's CMS mechanics group have no trouble analytically assessing the weights of designs or the radiation-lengths of assemblies. Accurately estimating the thermal performance of a complicated assembly using pen and paper, however, poses great challenges. Not only can certain variables only be determined experimentally, such as the heat lost to air and the effective thermal contacts between parts, but complicating factors of heat transfer in three dimensions and unusual thermal behaviors of certain materials (like anisotropy of thermal conductivity) make even an idealized estimation almost impossible.

As an alternative approach, the mechanics group also explored the use of an industrial-level thermal simulation software called ANSYS®. This too fails to produce a fully realistic estimate of the thermal performance of an assembly, but can be used to assess the relative thermal performances of various designs. Unfortunately, while very well suited for large-scale fixed designs, this simulation software works poorly for early-stage thermal evaluations. This unsuitability arises from the inflexibilities of the software and its closed-source nature. For every altered geometric parameter, en entirely new assembly file must be imported to ANSYS® and it must undergo a lengthy "meshing" process to create elements for finite difference approximations. This meshing process is unpredictable and can often lead to numerical errors when small features are present (even ones that are insignificant to thermal performance). In addition to this, incorporating non-traditional temperature dynamics, freely parameterizing thermal variables, and extracting specialized output variables at best requires creating auxiliary programs and at worst is made impossible by the software. With so many constraints and a steep learning curve, this too becomes unfeasible even for comparative evaluations of thermal performances of designs.

Of course, experimentally testing every conceptual design would make the detector assembly design very slow and costly, even given the group's possession of a liquid CO_2 source and a thermal camera. Thus, addressing the problem of thermal viability requires modeling of some form. The importance of this modeling for thermal evaluation paired with the difficulties encountered by the group with analytical calculations and industrial software yields a demand for an intermediate tool for thermal evaluation. This tool would need to be based on first principles, completely alterable, flexible in parameters, and capable of numerically simulating complex heat flow dynamics though unusual materials. This thesis outlines the

development of such a thermal tool and demonstrates results obtained from using the tool to tackle real design questions that currently pose as obstacles to the group's convergence on a final detector design.

After this introduction chapter, the thesis discusses how one can simulate thermal dynamics from first principles using finite difference approximations paired with pixel elements. This chapter on numerical simulations includes methods to simulate component boundaries, heat sources and sinks, and heat through materials with temperature-dependent and anisotropic thermal conductivities. From here, the document includes a chapter addressing the computational nuances of thermal simulations, specifically how to choose time and length steps for approximations and how to ensure computational efficiency. With the mathematical fundamentals and approach of execution established, the thesis delves into the implementation of the specific design problem at hand. It specifically discusses the hardware constraints involved in the forward pixel detector design and the use of the simulation tool for evaluation. After this, the thesis includes the results of three design evaluations. These involve the incorporation of adhesives and material layers into the design, the choice of foam-type and tubing diameter, and the effects of strategically cutting down on foam. This chapter also comments on the observed performance of the simulation tool. Finally the thesis includes a discussion of the strengths and drawbacks of the tool, the types of uncertainties encountered when approaching the problem, and the likely future uses of the tool presented, both in the short and long-run by Cornell's CMS mechanics group and, potentially, by other detector mechanics groups.

Chapter 2

Numerical Simulations

2.1 Simulating Heat Flow

This section addresses the use of fundamental thermodynamic principles to yield a step-wise algorithm that allows for the simulation of heat flow. The algorithm relies on finite-difference approximations along three dimensions and along time. This section addresses how the numerical algorithm reflects general heat flow and that when vacuum boundaries and heat sources and sinks are present. It discusses the rationale by which approximations are made, how to ensure the numerical stability of the algorithm, and addresses the computational efficiency of the numerical algorithm delineated. This method was inspired largely by the author's own coursework and by online lecture notes from Professor Adam Powell at WPI [Powell MIT].

2.1.1 Numerically Stable Finite Difference Approximations Heat Equation from First Principles

The heat equation, assuming no radiogenit heat production, takes the form

$$\frac{\partial}{\partial t}T(\mathbf{x},t) = \alpha\nabla^2 T(\mathbf{x},t), \qquad \alpha = \frac{k}{\rho c_p}, \tag{2.1}$$

where $T(\mathbf{x},t)$ is the temperature at some position and time and k, ρ, and c_p represent the thermal conductivity, density, and specific heat capacity of the material at the position and time $(\mathbf{x},t)$. α is called the thermal diffusivity. For a generalized function $f(x)$, one can use Taylor's theorem to make the approximation

$$f(x_i+\Delta x) = f(x_i) + \Delta x\frac{\partial f}{\partial x}\Big|_{x_i} + \frac{(\Delta x)^2}{2}\frac{\partial^2 f}{\partial x^2}\Big|_{x_i} + \frac{(\Delta x)^3}{6}\frac{\partial^3 f}{\partial x^3}\Big|_{x_i} + \dots \tag{2.2}$$

$$\begin{aligned}\implies \frac{\partial f}{\partial x}\Big|_{x_i} &= \frac{f(x_i+\Delta x)-f(x_i)}{\Delta x} - \frac{\Delta x}{2!}\frac{\partial^2 f}{\partial x^2}\Big|_{x_i} - \frac{(\Delta x)^2}{3!}\frac{\partial^3 f}{\partial x^3}\Big|_{x_i} + \dots \\ &\approx \frac{f(x_i+\Delta x)-f(x_i)}{\Delta x} + \mathcal{O}[\Delta x].\end{aligned} \tag{2.3}$$

This result is called a "forward difference approximation." A "backward difference approximation" would involve substituting $f(x_i+\Delta x)-f(x_i)$ in the approximation above with $f(x_i)-f(x_i-\Delta x)$. At the limit of $\Delta x \to 0$, these will be identical. Since $\Delta x \neq 0$, however, the strongest estimate of the first partial derivative of $f(x)$ at x_i arises from averaging the forward and backward difference approximation to obtain a "central difference approximation,"

$$\frac{\partial f}{\partial x}\Big|_{x_i} \approx \frac{f(x_i+\Delta x)-f(x_i-\Delta x)}{2\Delta x}. \tag{2.4}$$

Through a similar process, one can derive a expression for the approximation for the second partial derivative of $f(x)$ at x_i. This begins by adding together the Taylor series of $f(x_i+\Delta x)$ and $f(x_i-\Delta x)$ to obtain

$$f(x_i+\Delta x)+f(x_i-\Delta x) = 2f(x_i) + 2\frac{(\Delta x)^2}{2!}\frac{\partial^2 f}{\partial x^2}\Big|_{x_i} + 2\frac{(\Delta x)^4}{4!}\frac{\partial^4 f}{\partial x^4}\Big|_{x_i} + \dots \tag{2.5}$$

$$\implies \left.\frac{\partial^2 f}{\partial x^2}\right|_{x_i} = \frac{f(x_i+\Delta x) - 2f(x_i) + f(x_i-\Delta x)}{(\Delta x)^2} + \left.\frac{(\Delta x)^2}{12}\frac{\partial^4 f}{\partial x^4}\right|_{x_i} + \dots$$
$$\approx \frac{f(x_i+\Delta x) - 2f(x_i) + f(x_i-\Delta x)}{(\Delta x)^2} + \mathcal{O}\left[(\Delta x)^2\right]. \tag{2.6}$$

One can apply these approximations to equation 2.1 to construct a finite difference approximation for the progression of the heat equation through space and time. While it is obvious to use equation 2.6 for the spatial component, an optimal approximation requires determining the next temperature distribution in time from the temperature distribution before it. This means the forward approximation for the single derivative (equation 2.3) is preferable to the generally more robust central approximation (equation 2.4). This mix of approximations for functions in space and time is known as the "forward time, centered space" approach. For the case of temperature along one dimension, $T(x,t)$, the approximation for the heat equation at $x = x_i$ and $t = t_m$ would take the form

$$\frac{T(x_i, t_m+\Delta t) - T(x_i,t_m)}{\Delta t} + \mathcal{O}[\Delta t]$$
$$= \alpha\left(\frac{T(x_i+\Delta x, t_m) - 2T(x_i,t_m) + f(x_i-\Delta x, t_m)}{(\Delta x)^2} + \mathcal{O}\left[(\Delta x)^2\right]\right). \tag{2.7}$$

Excluding higher order terms, this means

$$T(x_i, t_m+\Delta t) \approx T(x_i,t_m) + \frac{\alpha\Delta t}{(\Delta x)^2}\left[T(x_i+\Delta x, t_m) - 2T(x_i,t_m) + T(x_i-\Delta x, t_m)\right], \tag{2.8}$$

ignoring higher order terms. Now, by defining $r \equiv \alpha\Delta t/(\Delta x)^2$, one can rearrange terms to write

$$T(x_i, t_m+\Delta t) \approx r\left[T(x_i+\Delta x, t_m) + T(x_i-\Delta x, t_m)\right] + (1-2r)T(x_i,t_m). \tag{2.9}$$

For compactness and ease of notation for higher dimensions, I will denote $T_i^m \equiv T(x_i,t_m)$ and $T_{i\pm1}^{m\pm1} \equiv T(x_i \pm \Delta x, t_m \pm \Delta t)$. In this notation, equation 2.8 becomes

$$T_i^{m+1} \approx r(T_{i+1}^m + T_{m-1}^m) + (1-2r)T_i^m. \tag{2.10}$$

In this notation, one can more compactly generalize to three dimensions with the extensions to the subscript of T, $y_j \pm \Delta y \equiv j \pm 1$ and $z_k \pm \Delta z \equiv k \pm 1$. This generalization entails adding terms for y and z to the equation 2.6. Along the x-dimension, equation 2.8 can be written as

$$T_i^{m+1} \approx T_i^m + \alpha \Delta t \left(\frac{T_{i+1}^m - 2T_i^m + T_{i+1}^m}{(\Delta x)^2} \right). \tag{2.11}$$

In three dimensions this becomes

$$\begin{aligned} T_{i,j,k}^{m+1} \approx T_{i,j,k}^m &+ \alpha \Delta t \frac{T_{i+1,j,k}^m - 2T_{ijk}^m + T_{i-1,j,k}^m}{(\Delta x)^2} \\ &+ \alpha \Delta t \frac{T_{i,j+1,k}^m - 2T_{ijk}^m + T_{i,j-1,k}^m}{(\Delta y)^2} \\ &+ \alpha \Delta t \frac{T_{i,j,k+1}^m - 2T_{ijk}^m + T_{i,j,k-1}^m}{(\Delta z)^2}. \end{aligned} \tag{2.12}$$

To simplify further, equation 2.12 requires the condition $\Delta x = \Delta y = \Delta z$. Calling this difference Δd, one can redefine $r \equiv \alpha \Delta t / (\Delta d)^2$. With this condition and grouping of terms, equation 2.8 becomes

$$\begin{aligned} T_{i,j,k}^{m+1} &\approx T_{i,j,k}^m + \frac{\alpha \Delta t}{(\Delta d)^2} \left(T_{i+1,j,k}^m + T_{i-1,j,k}^m + T_{i,j+1,k}^m + T_{i,j-1,k}^m + T_{i,j,k+1}^m + T_{i,j,k-1}^m - 6T_{ijk}^m \right) \\ &\approx r \left(T_{i+1,j,k}^m + T_{i-1,j,k}^m + T_{i,j+1,k}^m + T_{i,j-1,k}^m + T_{i,j,k+1}^m + T_{i,j,k-1}^m \right) + (1 - 6r) T_{i,j,k}^m. \end{aligned} \tag{2.13}$$

It is important to note that if the last terms of equations 2.10 and 2.13 for the one and three dimensional models, respectively, are negative, the iterated approximation can grow in amplitude and fail to converge. For this reason, it is necessary to choose $r < \frac{1}{2}$ for equation 2.10 and $r < \frac{1}{6}$ for equation 2.13 to ensure stability.

2.1.2 Boundaries and Varying Conductivity

The previous subsection includes a time-iterative finite difference approximation (equation 2.13) for temperature distributions under assumptions of a uniform ma-

terial and elements with neighboring elements on both sides along all dimensions. Of course, neither of these are true in the case of objects of finite dimensions and non-uniform compositions. A remedy to this requires special consideration to the r term in equation 2.13. One can begin by rewriting the equation as

$$\begin{aligned} T_{i,j,k}^{m+1} \approx T_{i,j,k}^{m} &+ r\left(T_{i+1,j,k}^{m} - T_{i,j,k}^{m}\right) + r\left(T_{i-1,j,k}^{m} - T_{i,j,k}^{m}\right) \\ &+ r\left(T_{i,j+1,k}^{m} - T_{i,j,k}^{m}\right) + r\left(T_{i,j-1,k}^{m} - T_{i,j,k}^{m}\right) \\ &+ r\left(T_{i,j,k+1}^{m} - T_{i,j,k}^{m}\right) + r\left(T_{i,j,k+1}^{m} - T_{i,j,k}^{m}\right). \end{aligned} \tag{2.14}$$

In this representation, it becomes clear that each r factor of every term represents the heat transfer between the spatially adjacent elements subtracted after it. For example, if $r = 0$ there is no temperature change. If r varies only in space, one can denote the value of r at (x_i, y_j, z_k) as r_{ijk}. The complete finite difference approximation where r varies then becomes

$$\begin{aligned} T_{i,j,k}^{m+1} \approx T_{i,j,k}^{m} &+ r_{i+1,j,k}\left(T_{i+1,j,k}^{m} - T_{i,j,k}^{m}\right) + r_{i-1,j,k}\left(T_{i-1,j,k}^{m} - T_{i,j,k}^{m}\right) \\ &+ r_{i,j+1,k}\left(T_{i,j+1,k}^{m} - T_{i,j,k}^{m}\right) + r_{i,j-1,k}\left(T_{i,j-1,k}^{m} - T_{i,j,k}^{m}\right) \\ &+ r_{i,j,k+1}\left(T_{i,j,k+1}^{m} - T_{i,j,k}^{m}\right) + r_{i,j,k-1}\left(T_{i,j,k+1}^{m} - T_{i,j,k}^{m}\right). \end{aligned} \tag{2.15}$$

One can write this more compactly as

$$T_{i,j,k}^{m+1} \approx T_{i,j,k}^{m} + \sum_{\ell \in S} r_{\ell}\left(T_{\ell}^{m} - T_{i,j,k}^{m}\right),\ S = \{[i \pm 1, j, k], [i, j \pm 1, k], [i, j, k \pm 1]\}. \tag{2.16}$$

Note that since Δt and Δd remain constant through simulations, r_{ijk} will vary only as α, defined in equation 2.1, varies. The time-iterative approximation of equation 2.15 makes it easy to encode spatial changes in r as material properties change. One can encode r as a preset spatial matrix along three dimensions.

Equation 2.15 also solves the challenge of encoding boundaries for simulations of finite dimensions. Consider, for example a simulation of heat in a rectangular

prism. At any element on a face, edge, or corner of the prism, not all six adjacent elements will exist. In the finite difference approximation, these elements will evolve according to equation 2.15 with the terms associated with the missing elements omitted. Rather than specifying these modified equations for each possible spatial condition, one can employ a "shell" approach, wherein additional elements are added completely surrounding the solid of interests and r at each element is set to zero. From here, one can iterate equation 2.15 exclusively to elements inside the shell and have the "missing" neighbors automatically omitted. While slightly less efficient computationally, this approach greatly reduces the amount of code otherwise needed to run the simulation, especially in the case of complex geometries.

2.1.3 Heat Generation for Power Sources and Sinks

Realistic thermal scenarios often involve heat sources and sinks where heat is generated or removed from a system. One can encode these by adding a term to the heat equation or by keeping temperatures at certain elements constant.

The latter can be achieved by encoding a spatial "mask" in the needed number of dimensions such that for some values the simulation applies equation 2.15 and, for other values, the simulation keeps the temperature constant. In three dimensions, this could take the form of a matrix $M_{ijk} \in \{0, 1\}$ where a value of 1 calls equation 2.15 and a value of 0 keeps the temperature constant.

In the case of constant power generation or dissipation, however, the solution involves more nuance. The full heat equation in the cases of non-zero heat gener-

ation is

$$\frac{\partial}{\partial t}T(\mathbf{x},t) = \alpha\nabla^2 T(\mathbf{x},t) + \frac{\dot{q}_v}{\rho c_p}, \tag{2.17}$$

where $\dot{q}_v$ is the volumetric heat generation with units of power density. From the approximations detailed in Section 2.1.1, it is clear that this modification would entail the addition of a term $\Delta t\dot{q}_v/(\rho c_p)$ to equation 2.8. Calling this term h^m_{ijk} for time m and spatial coordinates i, j, k, one can modify equation 2.16 to obtain

$$T^{m+1}_{i,j,k} \approx T^m_{i,j,k} + \sum_\ell r_\ell \left(T^m_\ell - T^m_{i,j,k}\right) + h^m_{i,j,k}, \tag{2.18}$$

where $\ell \in S$ is defined in the second part of equation 2.16. If the heat generation does not change with time, $h^m_{ijk} \to h_{ijk}$ and it can be encoded similar to r as a spatial matrix in three dimensions.

2.2 Dynamic and Directional Materials

This section delves into extensions of the thermal simulation algorithm presented in the previous section to encompass materials of unusual thermal properties. The two properties addressed are temperature-dependent thermal conductivity and directional (anisotropic) thermal conductivity. Materials in the current CMS forward pixel detector design exhibit both thermal behaviors, making these extensions necessary for accurate evaluations of thermal performances.

2.2.1 Temperature Dependent Conductivity

In the prior section it was assumed that the thermal conductivities of materials stay constant over the space they occupy. While not entirely true for certain rele-

vant materials like composites and those with grains and boundaries, microscopic spatial effects average out over tangible length scales and can be ignored. This is not the case, however, for changes in conductivity as functions of temperature. These effects alter both transient and equilibrium temperature profiles of assemblies undergoing thermal changes. Thus, the consideration of how conductivity levels change with temperature is an important one for effective simulations. This is especially true for assemblies with large distributions in temperatures and that contain temperature-sensitive materials.

The CMS pixel detector assembly contains such wide temperature distributions and such materials of temperature-sensitive conductivities: namely silicon and glass. For the case of glass, the change roughly follows the linear approximation

$$k(T) \approx 1.0143 + 3.57 \times 10^{-4} T$$

for temperatures of interest [van der Tempel *et al.*, 2000]. For silicon, the dependence in temperatures of interest takes the approximate form

$$k(T) \approx 165.406 - 0.625T$$

as shown by [Glassbrenner *et al.*, 1964]. [Wang *et al.*, 2008] Points to an effect on the thermal conductivity of individual carbon fibers with temperature, but this is not an appreciable change in the relevant temperature range and only affects in-plane conductivity (discussed in the next subsection).

When one can establish functional relationships between the thermal conductivity k of a material and its temperature T, finite difference simulations must be modified to incorporate the evolution of k along time. By the definition of α from equation 2.1 and the definition $r \equiv \alpha \Delta t/(\Delta d)^2$ from the previous section, it follows that changes in k are reflected (proportionally) as changes in r. Thus, through the

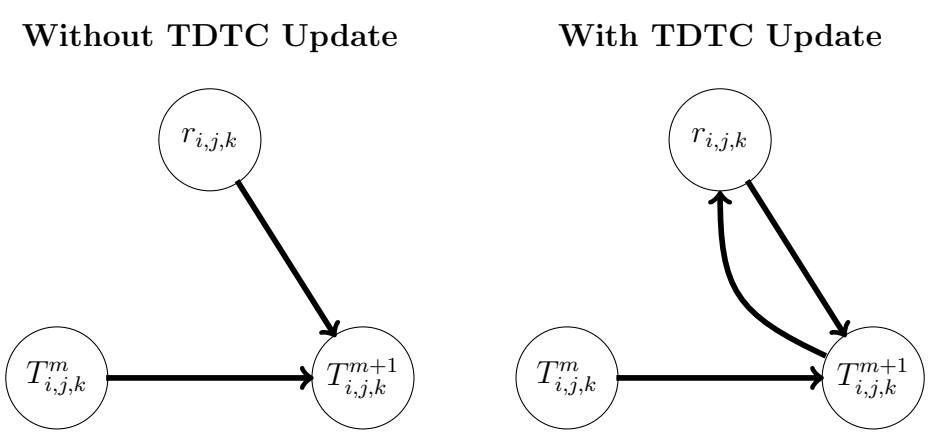

Figure 2.1: A schematic showing the influences between r and T in a finite-difference thermal simulation (equation 2.15) without temperature-dependent thermal conductivity (TDTC) considerations (left) and with them (right).

process of iteration long time, r must influence T, as before, but T must also influence r. Figure 2.1 shows the difference between the finite-difference process outlined in equation 2.15 and this modified approach as schematics of influence.

In an ideal scenario, this update in conductivity of a material would occur at every iteration. For the sake of computational efficiency, however, it is wise to only update the conductivity levels of each pixel after some number of iterations along time. This periodic, rather than continuous, updating serves as a good approximation due to the limited influence of small changes in temperature to changes in conductivity. In scenarios where the latter change is large relative to the former, skipping conductivity updates can alter the trajectory of a simulation unfavorably.

2.2.2 Anisotropic Conductivity

The great majority of materials in engineered rigid products, including common plastics and metals, contain no macroscopic directional properties. Thus, heat and electric currents moving through such materials face the same resistance regardless of the directions in which they flow. Other materials, however, including quartz [Midttomme *et al.*, 1998], diamond [Graebner *et al.*, 1992], and carbon-fiber [Tian, 2011] exhibit anisotropic thermal conductivities; this means the materials conduct heat better in some directions than in others. In the first two cases, this is because of the crystal structures of the materials. In the case of carbon fiber, the anisotropy arises form the composite nature of the material, i.e. that it is made of fibers aligned in directions constrained to a plane. Because the final design of the CMS Forward Pixel detector assembly will almost certainly incorporate carbon fiber and could even involve diamond films for heat spreading, discussed more in Chapter 4, anisotropy is an important consideration for the simulations in focus.

At the limit of the finite-difference approach detailed in the previous section, the only way to implement anisotropy for a pixel is through a "weighting" of the effective thermal conductivity levels of its six neighbors. This means that the temperature of a pixel no longer represents an unbiased average of the differences between its temperature and those of its six neighbors – two on either size along each of the three spatial dimensions. To simplify this weighting, one can make a safe assumption of uniform anisotropy within all materials. This means that the thermal conductivity of a material along a given direction is the same at all points in the material. Necessarily, this implies that the thermal conductivity of such a material must be the same in one direction as in the anti-parallel direction.

Thus, incorporating uniform anisotropy into a finite-difference thermal simulation involves determining the effective thermal conductivity levels k_i along three orthogonal directions: the basis coordinates of the simulation. Denoting these directions as x, y, and z, this means identifying a vector $\vec{k} = [k_x,\ k_y,\ k_z]$. By the definition of α from equation 2.1 and the definition $r \equiv \alpha\Delta t/(\Delta d)^2$ from the previous section, one can determine the anisotropic heat diffusivity vector $\vec{\alpha} = [\alpha_x,\ \alpha_y,\ \alpha_z]$ and, from this, a vector $\vec{r} = [r_x,\ r_y,\ r_z]$. The vector $\vec{\alpha}$ encapsulates the uniform material properties relevant to heat conductivity in all directions. The vector $\vec{r}$, on the other hand, reflects properties of finite difference approximations and is more useful in incorporated directly into the finite difference formula. Returning to the subscripts i, j, and k, corresponding to spatial dimensions, one can rewrite the vector $\vec{r}$ as $\vec{r} = [r^{(i)},\ r^{(j)},\ r^{(k)}]$. With this, one can introduce an appropriate anisotropy modification to equation 2.15 and write

$$\begin{aligned} T^{m+1}_{i,j,k} \approx T^m_{i,j,k} &+ r^{(i)}_{i+1,j,k}\left(T^m_{i+1,j,k} - T^m_{i,j,k}\right) + r^{(i)}_{i-1,j,k}\left(T^m_{i-1,j,k} - T^m_{i,j,k}\right) \\ &+ r^{(j)}_{i,j+1,k}\left(T^m_{i,j+1,k} - T^m_{i,j,k}\right) + r^{(j)}_{i,j-1,k}\left(T^m_{i,j-1,k} - T^m_{i,j,k}\right) \\ &+ r^{(k)}_{i,j,k+1}\left(T^m_{i,j,k+1} - T^m_{i,j,k}\right) + r^{(k)}_{i,j,k-1}\left(T^m_{i,j,k+1} - T^m_{i,j,k}\right). \end{aligned} \tag{2.19}$$

This alteration to the equation for updating the temperature of a pixel along one step of time allows for proper incorporation of anisotropy.

While numerically correct, it is important to note that the incorporation of an "anisotropy-vector," rather than fixed r-values, may introduce unnecessary computation when the method iterates over materials with isotropic thermal conductivity. For this reason, a more efficient method would be to use equation 2.15 for iterations at all pixels within one pixel of boundaries between isotropic and anisotropic materials (toward the isotropic side). For all other pixels, the use of equation 2.19 is more appropriate.

Chapter 3

Computation

3.1 Finite Difference Scaling and Material Data

As explained in Chapter 2, values of r in finite difference equations in three dimensions – such as equation 2.15 – must remain below 1/6 to ensure numerical stability. Given the definition $r \equiv \alpha\Delta t/(\Delta d)^2$, it is clear that only Δx and Δt, properties of the simulation rather than of materials, can be altered to accomplish this. As Δx reflects the pixel size and is often determined upon the construction of the simulation, the best parameter to tune to reduce r to appropriate limits is Δt, the finite-difference time scale. A smaller time scale necessarily means more computational power to find equilibrium temperatures. Thus, one should aim to maximize Δt while keeping r below 1/6.

Ordinarily, when materials exhibit isotropy in thermal conductivity and no temperature-dependent thermal conductivity, this entails finding the maximum

level of α among all materials in an assembly and fixing Δt from a given Δx such that the maximum r value is just below 1/6. With the more realistic mechanisms outlined in Chapter 2, however, this problem becomes more complex. For anisotropic materials with vectors $\vec{\alpha}$ rather than scalar α values, one must take the maximum α level to be the maximum within the vector. Accounting for material anisotropy in thermal conductivity in this way is straightforward, but materials with temperature-dependent thermal conductivities can have their α values accidentally "wander" above numerically stable values. Though this is not a present concern in the simulations performed in this thesis, it can be mitigated with periodic "checking" that no r-values surpass 1/6 – i.e. periodically searching through $r_{i,j,k}$ for violations.

As discussed in Chapter 5, the ratio of execution time to simulated time is important for evaluating the speed of this tool. This ratio not only depends on the computational power of the machine on which simulations are run, but also on the time steps of the simulations. For some α_{max} corresponding to a fixed maximum r-value, one can rewrite the equation defining r as $\Delta t \propto \alpha_{max}(\Delta d)^2$. This means that Δt increases linearly with α_{max} and as the square of Δd. Since higher Δt values correspond to fewer iterations along time for a fixed-length simulation, is is clear that simulations run faster when lower spatial resolutions are used and when the maximum thermal diffusivity is higher. Unfortunately, this relationship "punishes" more accurate geometric representations of assemblies with greater times required to complete simulations.

3.2 Computational Efficiency

Both the complexities of the fixed components of the assembly and the intended flexibility of the simulation tool justify the use of a finite-difference approach to evaluate the performances of detector assemblies. The complete algorithm required to accomplish this, however, includes nested loops along three spatial dimensions and one more along time. More so, the operations involved are arithmetic and difficult to numerically reduce for the sake of efficiency. Thus, while measures to increase the algorithm's efficiency can yield meaningful payoffs in time, few such measures exist.

With that said, one very effective approach to increasing computational efficiency is to ensure machine compiling. All code written to implement this thermal simulation tool is in Python. While strong in interpretability and flexibility, Python scripts generally take longer to run than their common counterparts JAVA® and C++ [Python]. The choice of this language for this tool was deliberate due to its strengths in all measures except for speed. This hurdle, however, can be overcome through the use of the Python package Numba. By translating Python code into optimized machine code, Numba increases the speed at which the described finite difference simulations run, helping reduce the time it takes to characterize thermal behaviors of different assemblies [Numba].

3.3 Code Repository

All code written for this thesis and each project is open source and can be found on github at (www.github.com/ArthurCampello/CornellThesis).

Chapter 4

Problem Implementation

4.1 Hardware Constraints

Although much of the design of the CMS forward pixels is still incomplete, certain elements of the the hardware involved in the assembly, specifically the materials used, the module composition, and the general detector structure, have been fixed by the CMS mechanics team. This section discusses known design features and constraints in more detail and provides insights into the specific questions the central thermal evaluation effort seeks to answer. Understanding these details is necessary for the interpretation of the data presented in Chapter 5.

4.1.1 Involved Materials

The selection of materials involved in the construction of the forward pixel detector include those that satisfy three semi-quantitative requirements: being relatively light, being low-Z and radiation hard, and being relatively inexpensive. Few materials jointly satisfy all three constraints to their ideal levels, meaning compromises exist. CVD (chemical vapor deposition) diamonds, for example, are very low-Z (since carbon is only the 6th element in the periodic table), lightweight, and have exceptionally high thermal conductivity of $\approx 2200\text{W}/(\text{mK})$ [Twitchen *et al.*, 2001]. However, the high cost of CVD diamond excludes it from the selection of materials outlined in this subsection.

The table below lists the materials currently considered for incorporation into the assembly. It includes the relevant thermal properties of these materials (with temperature dependence and vector anisotropy as described in Chapter 2 where appropriate). The table contains the sources for the data on each material. Note that the functional approximations for the thermal conductivities of glass and silicon as functions of temperature arise from linear approximations to curves shown in literature around temperature ranges of interest.

As discussed in Chapter 1, metals are generally not viable materials due to their low radiation lengths. One can note that no metals are present in the table aside from the aluminum in the aluminum nitride. This material is a highly-conductive ceramic that will likely be incorporated into the final detector design in small (volumetric) quantities, due to its high density.

	$k\ \left(\frac{W}{mK}\right)$	$\rho\ \left(\frac{kg}{m^3}\right)$	$c_p\ \left(\frac{J}{kgK}\right)$	Sources
Carbon Foam 1	10	90	180	A, (Internal Data)
Carbon Foam 2	29	190	180	A, (Internal Data)
Carbon Foam 3	75	350	180	A, (Internal Data)
Carbon Fiber	[15.7, 15.7, 0.687]	1578	887	A, (Internal Data)
Glass	$1.01 + 3.6 \times 10^{-4}T$	2600	840	B, (Internal Data)
Silicon	$165.41 - 0.63T$	2336	705	C, (Internal Data)
Al-Nitride	180	3310	750	D, (Internal Data)

Table 4.1: This table shows material data relevant to thermal conductivity for the selection of materials considered for use in the detector assembly. All materials listed are explored in the evaluations performed in Chapter 5. The last column lists the sources from which these data were obtained (designated as letters defined in this caption). For all materials, some quantities came from internal data from the CMS group. The source designations are as follows A: [Anghelescu , 2009], B: [van der Tempel *et al.*, 2000], C: [Glassbrenner *et al.*, 1964], D: [Precision Ceramics].

4.1.2 Module Structure

In the CMS Phase-II Forward Pixel detector assembly, the modules serve as the primary source of heat. As discussed in the introduction, much of the detector assembly is designed to ensure this heat-load does not compromise the detector. This is the motivation for the entire computational tool presented in this thesis as, otherwise, only structure would be a consideration and this would require no simulation. Because of its central importance to the problem in focus, it is necessary to reflect its features as accurately as possible in the simulation. Unfortunately, at the stage of development present to the writing of this thesis, the module designs are

not entirely fixed and may undergo revision. This fact helps justify a flexible evaluation tool like the one presented in this thesis. Thankfully, however, collaborators on this effort at Purdue University have designed a so-called "dummy module" that mimics the power load of a completed module. This model likely reflects properties of the complete module design once it is finalized and will serve as the basis for information about the "module" in this section. Figure 4.1 c) shows an ordinary image of this dummy module and Figure 4.1 b) shows a thermal infrared image taken of the dummy module when powered at a load of 2.5 Watts.

For the purposes of simulation, some assumptions are made about the module that deviate from reality but impart negligible effects on the simulation. The first of these is that the module is made of only silicon and glass. In reality, the module contains many wires that are integrated into circuits and some that are wire-bonded after the fact. Additionally, wire-bonds may be covered in some encapsulant for their protection and some electrical components may be laminated. These features are high in number, insignificant, and currently uncertain, meaning a simulation that reflects them would require much more effort to construct with little payoff in accuracy. Additionally, the fact that wires and laminates may conduct heat better than silicon and glass means that an approximation of omission of these features helps bias the result (slightly) in an unfavorable direction for conductivity. This helps ensure the simulation's purpose as a "worst-case" evaluation. Figure 4.1 a) shows the dimensions of the two module components under this assumption.

An important feature shown in the module and incorporated into the simulation tool is the uneven distribution of power dissipation. Specifically, the module includes a strip on its silicon surface that generates far more power than the rest of the module (which still generates some power). This strip comes in six segments

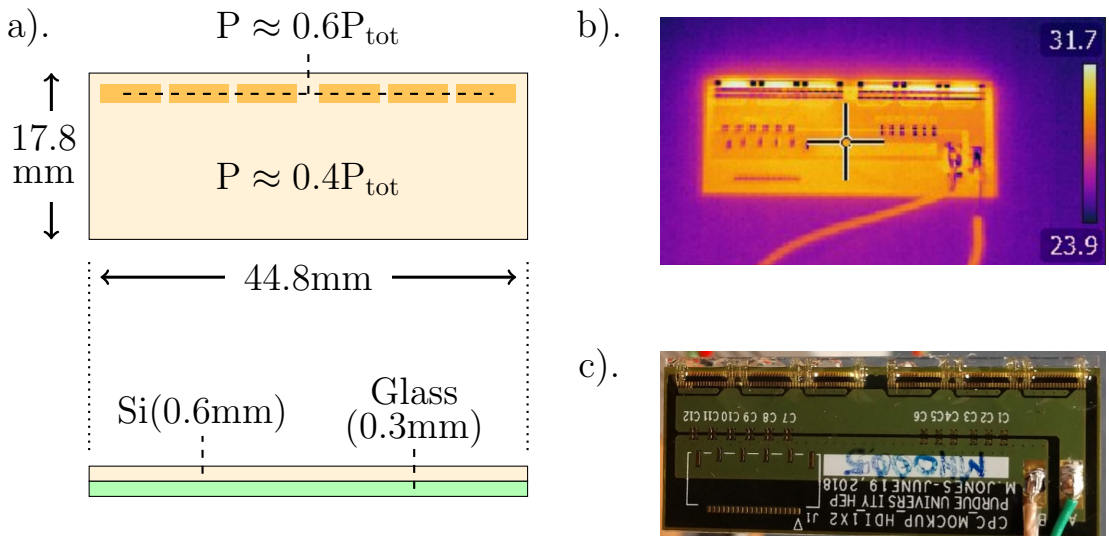

Figure 4.1: a) The dimensions of the main components of the modules (silicon in pale and glass in green) and a rough distribution of the power done by the shunts (darker pale) versus the rest of the silicon (pale). b) A thermal image take of a dummy module powered at 2.5 Watts in air showing its steady-state temperatures. c) An image of the dummy module showing its silicon component, the class, the leads, and the wire bonding.

known as "shunts" due to their relatively large heat dissipations. Features like these further justify the use of a numerical simulation tool over industrial software as the geometries of the shunts are not encoded in assembly files and would need to be done so (tediously) within the rigid framework of industrial software. Additionally, the simulation tool keeps the ratio of the total power generated to that generated by the shunts as a free parameter. quantifying this ratio as a single parameter is easier for users than requiring that they manually input the power generated by each individual shunt (performing manual calculations to account for the small volumes of the shunts).

4.1.3 Fixed Detector Structure

While much of the design for the CMS forward pixel detector remains uncertain, the CMS mechanics group at Cornell has converged on a base structure for the detector from which to extend other design decisions. Figure 1.2 of Chapter 1 shows this overall base design, which involves an antler-shaped cooling tube and semi-circular dees. In an ideal setting, the thermal viability of the detector would be evaluated at this full-dee level. Unfortunately, this entire assembly is too complex for the use of a finite difference simulation tool like the one proposed by this thesis.

The overall thermal quality of the design, however, depends mostly on the efficiency with which it can transport the heat generated by the modules to their nearest cooling tube sections in the dees. Thus, one can accurately evaluate designs by evaluating a smaller structure comprised of a single module on a section of the dee with two cooling tubes running under it. This structure is shown in figure 4.2.

It is from this base model that all thermal evaluations of alternative detector designs are evaluated; Chapter 5 contains the results of these evaluations. Only the dimensions shown in the figure (and relating to the module implicit in Figure 4.1) are known to be fixed. An exception to this is the tubing radius, which could be increased to 3mm. The effects of this coupled with the choice of foam from Table 4.1 are evaluated later in the thesis. The yellow region shown in Figure 4.2 represents any possible combinations of material layers or adhesives. It is also possible that the carbon fiber between the module and the foam will be substituted with an alternative material, such as aluminum nitride. The effects of such modifications are also evaluated in the next chapter.

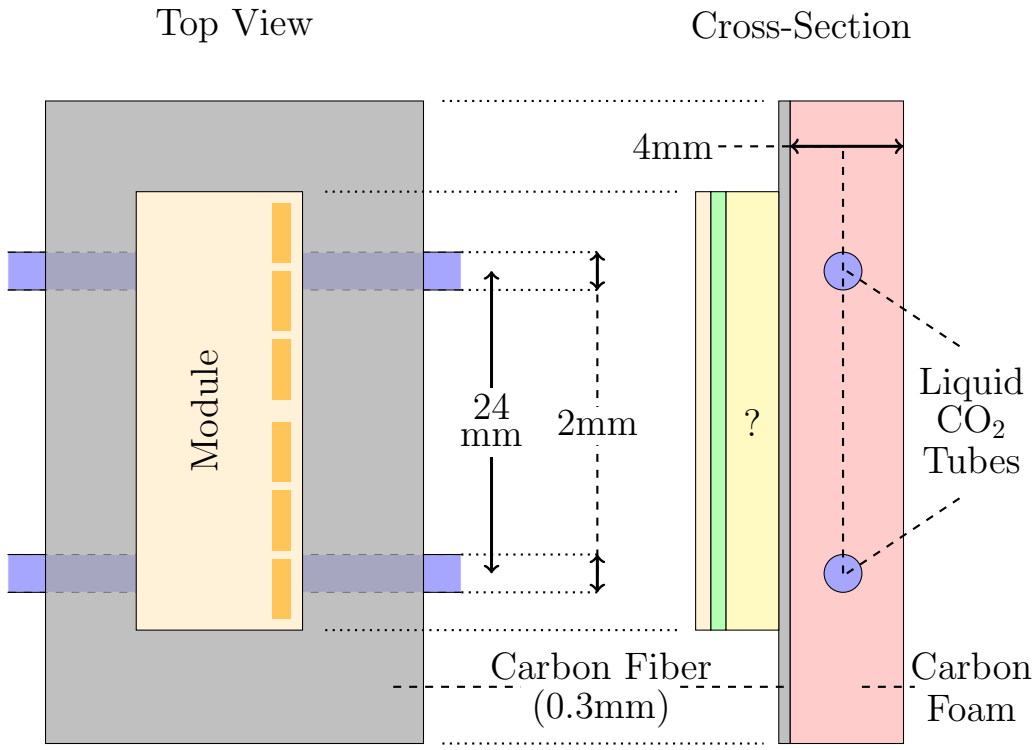

Figure 4.2: This shows the known detector assembly structure from top and cross-sectional views with the module assembly from Figure 4.1 a) included. All included dimensions are known while others are either arbitrary or unknown. The module components are shown in the same color as in Figure 4.1, carbon fiber is shown in gray, carbon foam in red, and the tubes containing liquid CO_2 in blue (the pipes will either be titanium or stainless steel). The question-marked yellow component represents the sub-assembly that connects the module to the rest of the detector assembly that must be optimized.

4.2 Evaluation Mechanism

Until now, only the ability of the tool to simulate heat flow dynamics has been discussed. Because the primary function of this tool is to evaluate various designs, some concrete evaluation mechanism must be determined. As discussed in Chapter 1, the primary concern of thermal viability involves the overheating of the silicon-tracker components, i.e. the module. Thus, one facet of the final evaluation metric must involve the average temperature of the silicon in the assembly. To

understand the dynamics of the silicon temperature over time, one can plot, for a single assembly design, the average silicon temperature over time for various input power levels. When doing so, three distinct outcomes arise: the power is small enough such that the silicon temperature eventually reaches that of the cooling tubes, the power is large enough such that that the temperature grows linearly with time, or the power level yields a steady-state temperature above that of the cooling tubes. Figure 4.3 shows these outcomes discretely.

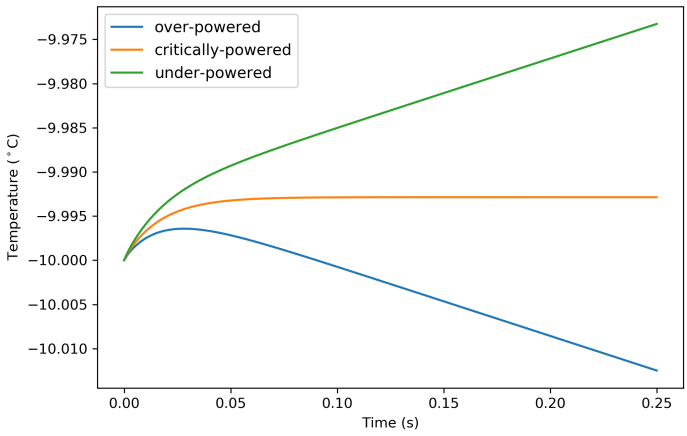

Figure 4.3: This figure shows the average silicon temperature over time for three simulations run with spatial resolutions of 300μm and 50 simulated millisecond conductivity updates for 0.25 simulated seconds for an assembly with 2mm diameter cooling tubes, 0.19g/cc foam, and the module directly on the carbon fiber. The blue line shows the "under-powered" scenario where the a power level is input such that the cooling tubes can effectively extract heat from the assembly. The green line shows the the "over-powered" scenario where a power level is input such that the assembly fails to extract heat efficiently enough and the silicon's temperature grows linearly. The orange line shows the "critically-powered" scenario where the power input to the module is at the highest level at with the silicon does not overheat.

From a numerical perspective, this means that, at some time after transient effects disappear, an overpowered system is characterized by a positive slope in the average-silicon-temperature over time plot. The outcome with a zero final slope is

that where the module is critically powered. The higher this "critical power" for an assembly, the more heat it can draw from the modules into the cooling tubes. Thus, the critical power serves as an evaluation metric for the **comparative** assessment of different thermal designs. While this critical power does not accurately reflect the true critical power of the modules, therefore, one can compare the simulated critical power levels of two designs and safely assess that the design with the higher one is more likely thermally viable.

To find this critical power in practice, one could use a numerical algorithm known as the bisection method for finding roots of functions. This is especially appropriate for finding the roots of strictly increasing functions with one root. Algorithm 1 shows how this numerical method works.

Algorithm 1 Bisection Method to Find g^* such that $f(g^*) = 0$

initialize $g_- \in \mathbb{R},\ f(g_-) < 0$
initialize $g_+ \in \mathbb{R},\ f(g_+) > 0$
while $f(g_0) \neq 0$ **do**
  $g_0 \leftarrow (g_- + g_+)/2$
  if $f(g_0) < 0$ **then**
    $g_- \leftarrow g_0$
  else
    $g_+ \leftarrow g_0$
  end if
end while
return g_0

The function in focus for this problem takes in a power level and outputs the slope of the average-silicon-temperature-over-time plot after some fixed time. The power level at which this output slope is zero corresponds to the critical power level. A natural lower bound input would be that of zero power (i.e. $g_- = 0$). At this power level, assuming the ambient temperature is above that of the cooling

tubes, the temperature of the silicon must decrease (or remain constant in cases of idealized zero-conductivity layers). From here, the output of the function can only increase as more power is added. Thus, it follows that the function in focus has exactly one root. Any power level such that the design is overpowered, therefore, serves as a good g_+ input.

This evaluation criterion and the bisection method were used to generate all the results included in the next chapter (Chapter 5). Although the bisection method converges quickly on the singular roots, each individual step in its loop takes a large amount of time as every evaluation of the function f requires an entire thermal simulation along time. Thus, it is advised to use intuition to select initial g_- and g_+ that more closely surround the root when it is approximately known. In addition, while a bisection method routine would ordinarily involves checks that $f(g_-) < 0$ and $f(g_+) > 0$, these are omitted as they each require time-intensive evaluations. It is also important to note that the implemented bisection method stops after some number of iterations instead of stopping after it meets some convergence criterion.

Chapter 5

Results

5.1 Design Evaluation

This section shows the results of several simulated experiments that demonstrate the relative effects of parameter alterations on thermal performances. As explained in Chapters 1 and 4, the results demonstrate relative rather than nominal measures thermal viability. All outputs are represented as "critical power" levels, as described in the second section of Chapter 4. Though these outputs should have units of Watts, they are represented as "arbitrary units" to avoid conveying the misleading notion that these represent true critical power levels that would be observed in experiment. Note that critical power levels may only be compared with those within the same simulated experiment as certain simulation parameters change their nominal values. Thermal performances may only be compared side by side if simulation parameters are kept consistent between them.

5.1.1 Carbon Fiber Substitution, Glues, and Contacts

Of primary concern to the thermal viability of the design are the relative effects of adding adhesives and layers between components. Unfortunately, measuring these effects numerically and at this stage of design poses challenges. As discussed earlier, the validity of the simulation tool presented in the thesis rests on the fact that even if the resistivities of these contacts are uncertain, they will affect all roughly-similar module assemblies in the same way. Thus, when a parameter is varied, the resistive contacts will alter the measures of thermal performance monotonically. The section titled "Uncertainties" in 6, discusses the uncertainties of thermal contacts in more detail. Due to the geometry of the assembly shown in Figure 4.2, it is clear that relative thermal outcomes of adhesives and layers used (denoted by a "?" in the figure) depends on their thermal resistivities and their thicknesses (on the assumptions of their relative overall small thicknesses and thermal isotropy). Thus, a thermal simulation tool is not of much use in determining which adhesives to use over which others. More so, it cannot quickly reproduce the relative benefit of an adhesive in providing better contacts as its simulations assume perfect contacts.

Despite this fact, the thermal simulation tool can still provide insights into the relative performances of different layerings of materials in different assemblies by keeping the resistivity of adhesives as a variable parameter. This can be accomplished by adding single-pixel-thick layers between components (and other material layers) and treating the resistivity of the pixel layer as that of an adhesive or that of a poor contact (i.e. where a part is held onto another without an adhesive). In the evaluation presented in this subsection, three assemblies involving "adhesion" layers are compared simultaneously while a single parameter proportional to the

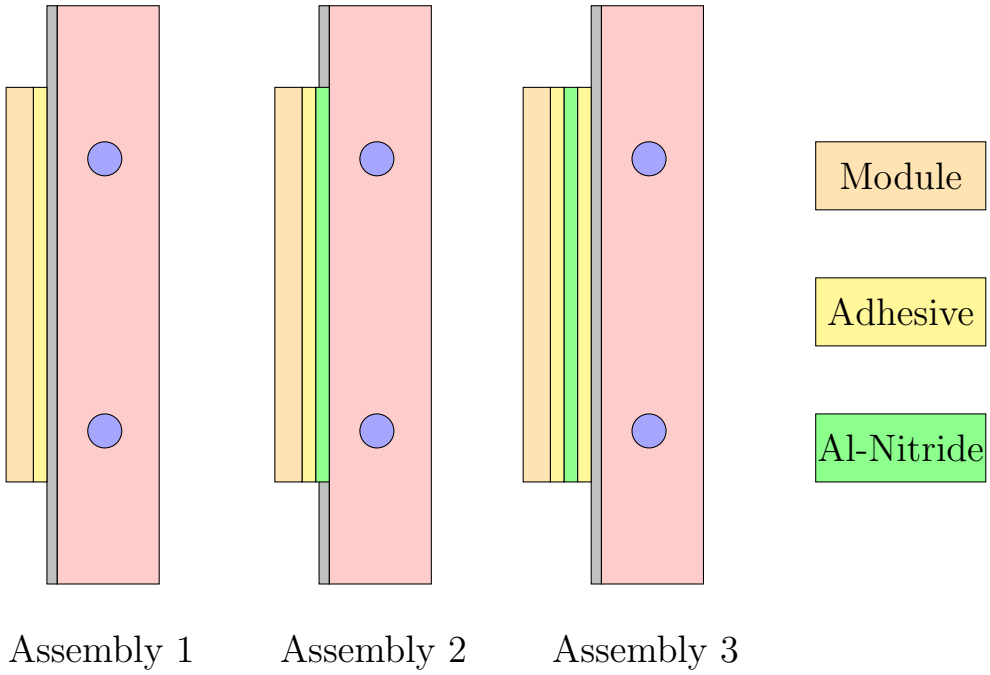

Figure 5.1: This figure shows three different assemblies that include adhesives (which may also represent thermal contacts with air gaps) between the module and the rest of the detector structure. The three represented assemblies are shown as cross-sections analogous to Figure 4.2 b) and with the same dimensions. The module is now shown as one continuous component in orange. The yellow components represent adhesive layers or thermal contacts, and the green components represent aluminum nitride layers. Due to the realistic thinness of these materials, all are represented as one pixel thick in simulations.

thermal diffusivity of a single type of adhesion is varied. Specifically, this parameter α is varied between 0 and 0.0001. Two assemblies involve the use of aluminum nitride either as a substitution for the carbon fiber, or as a layer placed on top of the carbon fiber; these two are compared to an assembly where the module is simply bonded to the carbon fiber. Figure 5.1 shows schematics of these three configurations. The use of aluminum nitride not only carries potential thermal benefits due to its strong thermal conductivity (see Table 4.1), but also serves as an electrically resistive layer between the module and the rest of the detector, which ensures stable electrical function.

The plot below shows the performances of these assemblies as a function of the α-value of the adhesive. At $\alpha = 0$, these lines are necessarily zero as the adhesives/contacts would conduct no heat. A vertical line corresponding to the thermal diffusivity of aluminum nitride is included for reference. It is important to note that adhesives hold the carbon foam to the carbon fiber and the carbon foam to the cooling tubes. As these affect all simulations uniformly, the outcomes of the simulations still serve well for comparative evaluations.

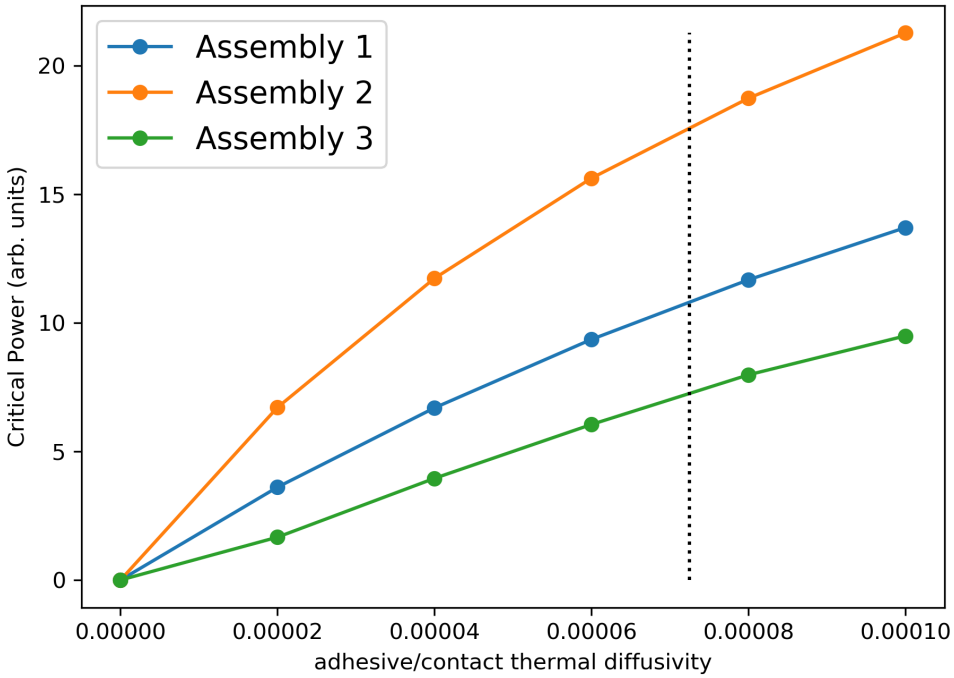

Figure 5.2: This plot shows the relative thermal performances of the three assemblies shown in Figure 5.1 with the thermal diffusivity of the adhesive layers (or the effective diffusivity of a thermal contact) as an independent parameter from 0 to 0.0001. Each individual simulation was run for 0.35 simulated seconds at 50 millisecond temperature-dependent conductivity, a 300μm spatial resolution, 2mm diameter tubes, and 0.19g/cc foam. The vertical black line shows the thermal diffusivity of aluminum nitride for reference.

From the plot, it is clear that Assembly 2 performs the best among the assem-

blies and Assembly 3 performs the worst for all measured levels of thermal diffusivity α. The fact that Assembly 1 performs better than Assembly 3 is unsurprising as the only difference between the two is that the latter has more layers than the former. The fact that Assembly 2 outperforms Assembly 1 is somewhat surprising, however, due to the high in-plane conductivity of the carbon fiber shown in Table 4.1. The benefit to replacing the carbon fiber with aluminum nitride likely arises from the superior conductivity of aluminum nitride compared to the through-plane conductivity of the carbon fiber. As assembly 2 contains both aluminum nitride (as a needed electrically resistive layer) and realistic bonds, it serves as a strong candidate for the optimal assembly among the three for thermal viability.

5.1.2 Foam-Type and Tubing Diameter

Two significant parameters of the CMS forward pixel detector design that have not been fixed by the current design are the tubing diameter of the pipes carrying the liquid CO_2 and the density of the carbon foam used. The tubing diameter is expected to be either 2mm or 3mm and the form density will correspond to one of the three types listed in Table 4.1 in the previous chapter. Given the thermal parameters shown for the types of carbon foam, namely the positive correlation between density and thermal diffusivity, it is likely that more dense foams will perform better (i.e. yield higher maximum power ratings) than less dense ones. Using a denser foam, however, is not strictly preferable as it means a more massive final product. The tubing diameter has a less straightforward expected effect on thermal performance as wider tubes lead to less uniform temperatures at the contact surface between the module and the carbon fiber.

The table below shows the results of thermal assessments ran for a simulated

0.35 seconds, on an assembly with no layers between the module and the carbon fiber, with temperature-dependent conductivities updated every simulated 50 milliseconds. These simulations assess the performances of designs with all combinations of 2mm or 3mm tubing and carbon foams of densities 0.09, 0.19, and 0.35 g/cc (grams per cubic centimeter). As discussed in the previous chapter, the outputs of these tests are in arbitrary units representing maximum power. Because this assessment tests along two parameters, it gives insights into the relative magnitudes of their impacts on thermal performance.

$\epsilon = \pm 10^{-7}$	0.09g/cc Foam	0.19g/cc Foam	0.35g/cc Foam
2mm ⌀Tubing	0.1928203	0.1929120	0.1929185
3mm ⌀Tubing	0.1928685	0.1929022	0.1929081

Table 5.1: Results of thermal evaluations of design evaluations of assemblies with tubes with 2mm and 3mm diameters and foam densities of 0.09, 0.19, and 0.35 g/cc. These simulations were run for 0.35 simulated seconds, with thermal conductivity updates at every simulated 50 millisecond-interval. The spatial resolution used was 300μm.

In relative terms, comparisons along the rows of the table show the anticipated results. The thermal performance of the assembly appears to improve with increasing foam density for both tubing diameters. Notably, however, the performance improves more dramatically between the least dense and intermediately-dense foam than between the intermediate-density and most dense foam.

Interestingly, the effect of a increasing the tubing diameter from 2mm to 3mm appears to change with the density of the foam. For the 0.09g/cc foam, increasing the tubing diameter appears to increase thermal conductivity. For the other two foam-types, however, the opposite effect is observed. These observations appear

to show that for a foam of lower conductivity, the benefit of the increased contact with the wider constant-temperature tube offsets drawbacks from a lack of thermal uniformity at the module surface. For the two more dense foams however, the latter negative effect appears to outweigh the former positive one.

Across the entire Table 5.1, the best reported performance is for an assembly using a 0.35g/cc foam and a 2mm tubing diameter. Relative to the differences between this performance rating and others, however, the assembly with 0.19g/cc foam and a 2mm tubing diameter presents as a close second. Because this combination is shown to be jointly the second best in thermal performance and the second-best in weight (assuming 3mm diameter tubes are overall lighter than 2mm diamater ones), the 0.19g/cc foam and a 2mm tubing diameter appears to be the optimal foam and tubing combination.

5.1.3 Strategic Foam Removal

In the current design of the detector, the foam is assumed to be milled from continuous sheets of the size of a single "dee" as shown in Figure 1.2. While efficient in terms or production, foam used in this way comprises a large fraction of the total cost to produce the detector (and, by extension, to test it). One could consider a cheaper alternative where smaller pieces of foam are created such that they cover the cooling tubes with some lateral thickness. This could be made out of discrete pieces that are later assembled into the design. Assembly of the detector using such a foam arrangement would be more challenging, but the total amount of foam purchased would decrease as would the amount of foam used in the final assembly, reducing the cost and weight of the detector.

Before considering the merits and drawbacks of such an idea on the production side, one would need to evaluate whether reducing the foam to cover portions of the detector only along the tube would remain thermally viable. While the foam serves as one of the best conductors of heat among the selected materials in Table 4.1, one could argue that the high in-plane conductivity of the carbon fiber, characterized by its anisotropy vector, could successfully transport heat from the module to the areas in the "dee-plane" covered by foam.

As mentioned, while the tool presented by the thesis cannot nominally evaluate the steady-state temperature from each foam arrangement used, it can demonstrate the relative performances of designs as more foam is removed from the assembly. Specifically, the simulation tool allows the flexibility of altering a parameter representing the "lateral-width" of the foam if it is assembled in the form of rectangular prisms centered at the cooling tube. Figure 5.3 b) below shows a representation of this parameter. When it is zero, there is no foam, and the thermal performance is necessarily rated to be zero. At some critical width (specifically that corresponding to the distance between the tubes), the foam-removed design is equivalent to that of a dee completely filled with foam. I will call this with p^*. Figure 5.3 a) shows a plot of the simulated performance of a design – with nothing between the module and the carbon fiber – varied with the foam-width parameter p. The vertical line p^* represents the critical width. In theory, this line would be bounded between two scenarios: one where the in-plane conductivity of the carbon fiber does nothing to bypass the reduced thermal flow between the module and the tubes and another where this in-plane conductivity completely circumvents the heat-transfer otherwise conducted through the foam and no notable effect is seen. The former scenario is represented by the red dashed line in Figure 5.3 a) and the latter by the green one. These represent the worst and best-case scenarios of the effect of

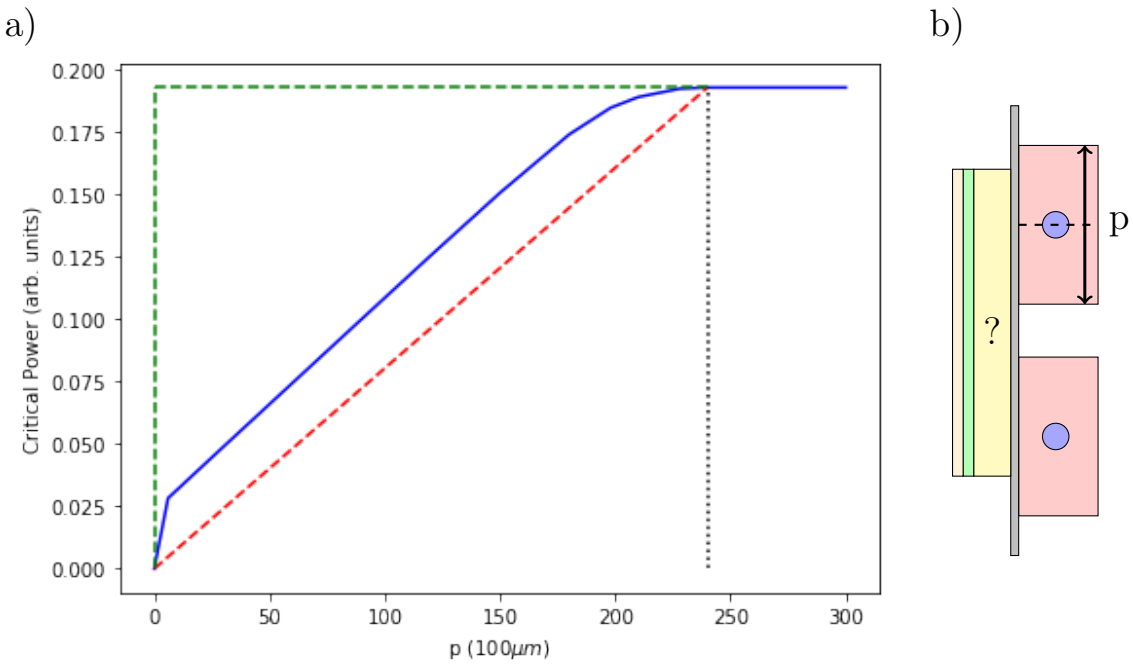

Figure 5.3: a). This shows plots of corresponding to worst-case, best-case, and measured thermal behaviors as a function of a parameter representing the in-plane width of foam perpendicular to the cooling tubes. The red dashed line shows the worst case scenario (that if the carbon fiber's heat spreading were zero), the green dashed line shows the best-case scenario (that if the carbon fiber's heat spreading were perfect), and the blue line shows the result measured from simulations run for 0.5 simulated seconds at 50 millisecond temperature-dependent conductivity, a 300μm spatial resolution, 2mm diameter tubes, and 0.19g/cc foam. The vertical black dotted line represents $p = p^*$, where p^* corresponds to the foam with at which the entire carbon fiber is covered. b). This shows a visual representation of the spatial parameter p with a cross-sectional diagram analogous to that from Figure 4.2 b).

spreading by the carbon fiber.

From the plot in the figure, it is clear that the heat spreading effect enabled by the high in-plane conductivity of the carbon fiber does relatively little to overcome the thermal barrier imposed by the removal of carbon foam. This is shown by the fact that the blue line strays closer to the worst-case scenario outcome than the best-case scenario outcome. For small gaps (i.e. high values of the parameter p)

the effect is negligible. At approximately $p = 175\mu$m, however, the outcome begins to more closely-mirror the worst-case.

This result indicates that only a minimal amount of foam-removal is feasible without compromising the thermal performance. At this small amount, it is likely that very little is saved in money and weight by removal of the material. Additionally, the complexity of handling multiple pieces of foam during assembly rather than one piece is likely to add costs. Thus, this simulation indicates that cutting down on foam in the way proposed will likely not strengthen the design while done to a degree that does not adversely affect its thermal performance.

5.2 Simulation Performance

Generally, very few problems arose from running the simulations involved in producing the results for this thesis. No crashes occurred and, given the error messages built in, no numerical issues were encountered. The main pitfall of the algorithm is the slow speed at which is runs. Even with efforts to mitigate this problem – outlined in Chapter 3 – individual simulations along time would take on the order of several minutes to run. For small-step iterations, this translated to many hours.

The best way to quantify the algorithm's overall performance on a given machine is to record the ratio of execution time to simulation time. This ratio arises from dividing the time it takes to run an individual simulation by the time simulated – e.g. if a simulation of an event spanning one second takes 100 seconds to run, the ratio is 100. Of course, this depends on many parameters of the simulation (most notably the spatial resolution in the case of this tool) and the computing

power of the machine running the simulation. Reporting these times for expected parameter sets when the simulation is run an ordinary personal computer, however, gives an intuition for the efficiency of the code. On average, across all simulations ran with the same spatial resolution (0.3μm) and the same conductivity update frequency (50 simulated milliseconds), I found this ratio to be approximately 166$\pm$8 executed seconds per simulated second. While this ratio would ideally be smaller – and would likely be if the tool us used on a faster computer – it is at a level where meaningful simulations can be performed within the average attention span.

Chapter 6

Discussion

This chapter includes discussions regarding the overall assessment of the simulation tool in addressing the problem central to the thesis, the uncertainties present in the problem and how the tool may help quantify and resolve these, and the future research directions involving the tool – both within and possibly outside the CMS mechanics group at Cornell. Because the results of simulations performed by the tool involve independent investigations with few joint conclusions, I relegate discussions of the results of each to their appropriate sections in the previous chapter.

6.1 Strengths and Drawbacks

The primary strengths of the simulation tool presented are outlined in the "Introduction" chapter and demonstrated in subsequent chapters. These include flexi-

bility of parameters, numerical stability, predictable completion time, and ease of substantial modification.

The first of this list is among the most critical for a streamlined evaluation of thermal designs and concepts. With an alternative thermal simulation software, such as ANSYS®, certain geometry-related parameters that are not explicitly defined in assembly files can be cumbersome to modify for a single iteration. For the problem at hand, such parameters notably include those that define the power dissipation profile of the module. More importantly, "scanning" over multiple parameter values to yield a summary of the effects of one parameter when others are kept equal is often difficult if not impossible with industrial software. As most rely on imported CAD assemblies, auxiliary programs would be necessary to accomplish this. In the case of the titular tool, one can implement loops over parameter values or comparatively evaluate sets of parameters with relative ease. Similar to the ease at which users of the presented simulation tool may alter input parameters is that with which they may define an output parameter (or set of parameters) for the purposes of evaluation. For the results outlined in the previous chapter, this output parameter represented the average temperature of the silicon comprising the module.

An additionally important benefit of the simulation tool presented is that of numerical stability. As outlined in Chapter 2, a maximum r-value of $1/6$ guarantees that the results represented will both avoid arbitrary divergences and numerical errors leading to software crashes. This is additionally guaranteed by the fact that the meshing is predetermined and cubic, meaning infinitely small faces – that are possible with automated meshing – do not pose numerical problems. From anecdotal experiences that I and my colleague Dr. José Monroy have had with

using ANSYS®, we know the software will often generate poor meshings that cause a series of complicated errors and may cause simulations to crash unexpectedly. The titular tool's strength of the absence of the possibility of crashing especially presents a benefit when simulations are set to run for long periods of unsupervised time – for example, overnight.

Paired with this benefit of stability is that of a predictable completion time. The auxiliary methods and uncertain meshing present in industrial software such as ANSYS® make the time lengths required to complete a simulation unpredictable; these software often fail to represent cogent time to completion estimates as well. The tool presented, however, requires a definite time to complete proportional to the input parameters as specified in Section 1 of Chapter 3.

The final strength of the presented tool arises from the ease with which one can implement substantial modifications to it. Because the tool is designed from first principles and completely open source, one can incorporate features into it which may be difficult or impossible to in close-sourced software. As examples, one could implement materials with jointly anisotropic and temperature-dependent thermal conductivities, temperature-dependent heat sinks and sources, components with time-varying or position-varying fixed temperatures (as is likely the realistic case with the tubes present in the design in focus), and materials of non-uniform anisotropy. This quality becomes more uniquely appealing to the thermal tool presented as materials and components increase in thermal complexities or more is precisely known about their properties. Conditional on its continued use for thermal evaluation of the CMS forward pixels, the tool is likely to undergo such substantial modifications.

While limited, certain drawbacks are exhibited by the tool presented. The most

apparent among these is the fact that the computation involved is exhaustive and requires a long time to complete – even with speed provisions detailed in Chapter 3. This time is empirically evaluated in the previous chapter and its scaling with the parameters r and Δd are discussed in Chapter 3. Unfortunately, the times required to run simulations increase quickly with pixel resolution and are generally large (on the order of several minutes to hours) even with machine compiling techniques.

An additional drawback of the tool is that dimensional parameters must be hard-coded as numbers and cannot be input through an intuitive 3D modeling software. For the CMS Forward Pixel detector assembly presented, this is a minor inconvenience as all components are either rectangular prisms or cylinders whose dimensions and placements are characterized by no more than six numbers combined. For designs with parts of more complex geometries, however, managing many dimensional parameters in a non-visual way may become cumbersome. While the current version of the tool includes easy visualization for temperature and conductivity, one could readily modify it to show cross-sections or rough 3D images of individual parts to ensure appropriate dimensions.

6.2 Uncertainties

As with any complex thermal assembly, many uncertainties play roles in the ultimate thermal performance of the CMS detector in focus. Understanding which of these can be resolved or quantified and in what order is critical to creating a cogent prediction of the thermal viability of the final design before its experimental evaluation. Relevant to the problem faced by the CMS mechanics group for this design are four classes of uncertainty: those which are systematic and design-

specific, those which experiment can validate, those dependent on the placement of the module on the detector, and those on the scale of individual components.

Systematic and design-specific include uncertainties in the detector designs that affect all modules equally and arise from design parameters that are either not relevant to thermal performance or that will not be determined by the Cornell CMS mechanics group. A primary example of such an uncertainty is that arising from the unclear module design. In all likelihood, the thermal behavior "dummy" modules provided to the Cornell CMS group by the CMS group at Purdue University roughly reflects that of the final module. However, small uncertainties regarding the distribution of power dissipation in the module and the thicknesses of the materials comprising it can lead to wider uncertainties in the thermal outcomes of designs. A similarly important parameter involves the material from which the CO_2 tubes will be made. This decision, likely between stainless steel or titanium, carries implications for thermal performance, but will likely be made on the basis of cost and weight. Wile tested in Chapter 5, the thickness of the tubing may also fall into such a category. The results of the simulation tool showed the thermal effects of this radius to be minimal, meaning the decision of tubing-radius likely depends on the availability of resources and the weight of the final detector.

The next class of uncertainties involves those that one can resolve experimentally. In ideal cases, resolving these involves the introduction of parameters to the simulation tool that allow it to more accurately reflect the physical reality. Chief among these parameters is that representing the extent to which heat is lost in air. As explained in Chapter 2, the simulation relies on an assumption that the entire assembly is in a vacuum, i.e. that no heat is lost to anything other than a component of the assembly. Because the final detector will be in air, this is a flawed

assumption. To determine how to reflect this in the simulation tool, one could conduct an experiment in which an aluminum block is heated with an internal hating element and the steady-state temperatures on all of its sides are measured. Once could then introduce a heat-sink "component" into a simulation of a heated aluminum block such that the simulated equilibrium temperature matched the observed one. Determining this heat-sink parameter for all temperatures would allow the simulation tool to better reflect the physical reality of heat loss due to air[1]. It would be equally important, although more challenging, to experimentally resolve the additional uncertainty of the transmission of heat through contacts between unbonded materials. This is specifically important to evaluate for contacts between the module and carbon fiber and the module and aluminum nitride. Doing so can help establish the net effect of the tradeoff between better contact and more thermal resistivity when components are glued together. To optimally resolve any uncertainty in this category, one must first resolve all design related uncertainties to ensure that measured parameter reflect the realities of the final design.

Module placement uncertainties are likely limited, but still important to identify for a complete thermal evaluation. These uncertainties arise almost entirely from the CO_2 tubes under the module (with the exception of convection effects throughout the entire detector). The two relevant factors to these uncertainties are the positioning of the tubes relative to the modules and the effective fixed temperatures of the tube. The problem of the former can be readily seen in Figure 1.2, which shows modules placed on points along a semi-circle over a tubing shape that is semi-octagonal. This mismatch means that most of the tubing-positions will not precisely reflect that shown by Figure 4.2. The uncertainty caused by

[1]This experiment was planned for late March of 2020 but could not be performed due to the closure of Cornell University's campus because of the novel coronavirus. It remains to be performed as of the writing of this thesis.

the tubing temperature along the path of the CO_2 is more complicated and likely involves modeling fluid dynamics. Specifically, there exists a possibility that the CO_2 undergoes a phase transition within the tubing given that the liquid may heat up from exposure to the modules. In this case, the gaseous CO_2 may not successfully draw heat from modules over tube-sections near the end of the CO_2 path.

The final classification of uncertainty is that which is part-specific. Ordinarily, this type of uncertainty can be mitigated with careful fabrication, but this may not be the case for the CMS detector in focus. Variations in part and module dimensions are likely unimportant, but there may be possible variations in the carbon foam properties throughout the thin sheets that make up the detector and there may be variations across modules in heat generation. The former concern has arisen in group meetings as a possibility; specifically, there exists a potential non-uniformity within one continuous piece of foam as well as possible variations between different foam sheets. Experimentation has not yet revealed the degree to which this occurs. Uncertainty in the heat generation of modules arises from potential mistakes with wire-bonding (even if automated) and module assembly defects that lead to air pockets.

6.3 Future Directions

In the immediate future, the CMS Mechanics team at Cornell University will find use for this tool in evaluating the relative merits of design concepts. These will likely include decisions on whether to prioritize module heat spreading over through-plane conductivity, on where materials may be removed from the design

for benefits of cost and weight, and on which materials to use, among others. As this happens, factors of the design that are either not up to the mechanic group or not important to thermal viability, such as the finalized module design and the tubing material, will likely become less uncertain, allowing the group to refine their evaluations.

From this point, the simulations will become more realistic and can inform a selection of designs to which time and financial resources are devoted for experimentation. From experimentation, certain parameters not known to the simulation tool may be fixed to better reflect reality. This would likely entail focusing on the systematic uncertainties outlined in the previous section, including the thermal effectiveness of contacts between parts and heat lost to air. With enough sophistication, the simulation tool could reasonably approximate the observed thermal reality observed in individual-module laboratory settings. The use of a few cases of agreement between such a modified tool and experiment will likely provide enough confidence that the tool can reasonably estimate the performances of alternative designs. For this purpose, the ease or incorporating measured parameters into the tool enabled by flexibility– discussed in Section 6.1– is critical to its success in guiding the design process.

In its final stage of relevance to the CMS project, the simulation tool could serve a purpose in estimating thermal uncertainties of modules situated in different locations over the detectors. As discussed in the previous section, these include the positions of the tubes under the module and the temperature of the tubes under the module. Establishing how the thermal outcomes of each assembly vary with these conditions would allow for a benchmark with which to compare a full thermal simulation of the detector. Such a full simulation could be performed with

an industrial thermal simulation software if the design were finalized. Of course, challenges might arise with such a comparison, both because some parameters in the titular simulation tool may be difficult to integrate into the industrial software and because one would need to assume no thermal interaction between neighboring modules. Paired together, these simulations would likely provide satisfactory computational assurance of the thermal viability of the converged-on design.

Although the titular simulation tool was created specifically for the CMS forward pixel detector, it has the potential to play roles in the designs of detectors with similar thermal challenges. The current version of the tool is especially useful for designs comprised mostly of rectangular-prism-shaped components. With enough use and generality, it has the potential to save design teams the time and resources involved in evaluating designs through experimentation where industrial software fails. While mechanics groups may be tempted to avoid intermediate and "blocky" evaluation tools like the one presented, the experience of the Cornell CMS mechanics group and the results outlined in this thesis demonstrate that doing so can streamline the design process in the early stages.

Bibliography

[Anghelescu , 2009] Anghelescu ,M.S *Thermal and Mechanical Analysis of Carbon Foam* . PhD dissertation, Russ College of Engineering and Technology of Ohio University, 2009.

[CERN CMS] *CMS Detector*, CERN, https://cms.cern/detector (Accessed 10 May 2020).

[CERN LHC] *High-Luminosity LHC*, CERN, https://home.cern/science/accelerators/high-luminosity-lhc (Accessed 10 May 2020).

[Chatrchyan *et al.*, 2012] Chatrchyan et al. (2012) Observation of a new boson at a mass of 125 GeV with the CMS experiment at the LHC, *Physics Letters B*, **761**(1), 30-61.

[Contardo *et al.*, 2015] Contardo, D ., Klute, M., Mans, J., Silvestris, L., Butler, J. (2015) Technical Proposal for the Phase-II Upgrade of the CMS Detector, CERN Scientific Committee Paper, https://cds.cern.ch/record/2020886 (Accessed 10 May 2020).

[Glassbrenner *et al.*, 1964] Glassbrenner,C.J., Slack,G.A. (1964) Thermal Conductivity of Silicon and Germanium from 3deg K to the Melting Point, *Physical Review*, **134**, 1058–1069.

[Graebner *et al.*, 1992] Graebner,J.E., Jin,S., Kammlott,G.W., Herb,J.A., Gardinier,C.F. (1992) Large anisotropic thermal conductivity in synthetic diamond films, *Nature*, **359**, 401–403.

[Midttomme *et al.*, 1998] Midttomme,K., Roaldset,E. (1998) The effect of grain size on thermal conductivity of quartz sands and silts, *Petroleum Geoscience*, **4**(2), 165-172.

[Numba] *Numba makes Python code fast*, Anaconda, Inc., http://numba.pydata.org/ (Accessed 15 May 2020).

[Powell MIT] Powell, Adam. "Finite Difference Solution of the Heat Equation." Massachusetts Institute of Technology 22.091, dspace.mit.edu. Accessed 10 Aug. 2019

[Precision Ceramics] *Aluminum Nitride Engineering Properties*, Precision Ceramics, https://precision-ceramics.com/materials/aluminum-nitride/ (Accessed 11 May 2020).

[Python] *Comparing Python to Other Languages*, Python Software Foundation, https://www.python.org/doc/essays/comparisons/ (Accessed 10 May 2020).

[Tian, 2011] Tian,T. *Anisotropic Thermal Property Measurement of Carbon-Fiber/Epoxy Composite Materials*. PhD dissertation, University of Nebraska, Lincoln, 2011.

[Twitchen *et al.*, 2001] Twitchen, D.J., Pickles, C.S.J., Coe, S.E., Sussmann, R.S., Hall, C.E. (2001) Thermal conductivity measurements on CVD diamond, *Diamond and Related Materials*, **10**(3-7), 731-735.

[van der Tempel *et al.*, 2000] van der Tempel,L. Melis,G.P., Brandsma,T.C. (2000)Thermal Conductivity of a Glass: Measurement by the Glass–Metal Contact, *Glass Physics and Chemistry*, **26**(6), 606–611.

[Wang *et al.*, 2008] Wang,J.L., Gu,M., Ma,W.G., Zhang,X., Song,Y. (2008) Temperature dependence of the thermal conductivity of individual pitch-derived carbon fibers, *New Carbon Materials*, **23**(3), 259–263.